

## Strength and gas permeability of porous cordierite-mullite ceramics with different phase compositions and microstructures prepared by a pore-forming in-situ technique

Wen Yan\*, Nan Li, Yuanyuan Li, Jun Tong and Hao Luo

The Key State Laboratory Breeding Base of Refractories and Ceramics, Wuhan University of Science and Technology, Wuhan, P.R. of China

Seven porous cordierite-mullite ceramics with different phase compositions and microstructures were fabricated by a pore-forming in-situ technique. The phase composition, pore characteristics, strength and thermal shock resistance were investigated through X-ray diffractometry (XRD), scanning electron microscopy (SEM), and a microscopical measured method, etc. It was found that the porous cordierite-mullite ceramics have an apparent and interconnected pore structure; and the strength, the thermal-shock resistance and the gas permeability of the porous cordierite-mullite ceramics with different phase compositions and microstructures are rather different. Additionally, for the porous cordierite-mullite ceramics with an apparent and interconnected pore structure, the gas permeability mainly depends on the median pore size. A porous cordierite-mullite ceramic consisting of 25 wt.% cordierite and 71 wt.% mullite gave the best performance, which had a high porosity of 42.4%, an appropriate median pore size of 42.3  $\mu\text{m}$ , a high compressive strength of 37.7 MPa, a high thermal-shock resistance and a high gas permeability of  $4.68 \times 10^{-12} \text{ m}^2$ .

**Key words:** Porous cordierite-mullite ceramics, Microstructure, Phase composition, Strength, Gas permeability.

### Introduction

With the rapid development of the high temperature industry, serious environmental pollution has been caused by the emission of a lot of harmful high temperature flue gas, which severely restricted the further development of this industry. Direct application of high-performance, high-temperature porous ceramic filters is expected to be beneficial to the purification of high temperature dusty gas [1-2].

Porous ceramics have attracted extensive attention because they have potential applications as high temperature dusty gas filters, molten metal filters, and thermally insulating materials, etc [1-21]. With respect to filter materials, properties including strength, thermal-shock resistance, thermal-expansion coefficient and gas permeability etc are important criteria in the selection of a viable, durable, filter material [1-2]. Cordierite ( $2\text{MgO} \cdot 2\text{Al}_2\text{O}_3 \cdot 5\text{SiO}_2$ ) possesses a low thermal-expansion coefficient, excellent thermal-shock resistance and chemical stability at elevated temperatures, as well as a low cost [7-11], but the mechanical properties are poor [11-16]. Mullite ( $3\text{Al}_2\text{O}_3 \cdot 2\text{SiO}_2$ ) has a low thermal-expansion coefficient and good thermal-shock resistance as well as excellent mechanical and chemical stability [11-18]. The relatively poor mechanical properties of cordierite ceramics can be improved by adding mullite as a

reinforcing phase [11-16]. Thus, compared with porous cordierite ceramics, porous cordierite-mullite ceramics should have a higher strength and higher performance at elevated temperature; and compared with porous mullite ceramics, porous cordierite-mullite ceramics should have a lower thermal-expansion coefficient and a higher thermal-shock resistance.

Beside the phase composition, the pore structure of a porous ceramic used for filters should be considered, because the pore structure determines the gas permeability and strength of a porous ceramic. Isobe et al [19] prepared porous alumina ceramics with unidirectionally aligned cylindrical pores by an extrusion method, and the permeability of the sample having 39% porosity prepared using fibers with a diameter of 43  $\mu\text{m}$  as pore-forming agent was  $3.9 \times 10^{-13} \text{ m}^2$ . Yan et al. [9] fabricated porous cordierite ceramics with well-distributed interconnected pores through a pore-forming in-situ technique, and the permeability of the sample with a porosity of 40.3% and an average pore size of 23.3  $\mu\text{m}$  was  $2.31 \times 10^{-12} \text{ m}^2$ . Contrasting the two pore structures, it seems that a structure with well-distributed interconnected pores has a higher gas permeability. Additionally, the porosity and the pore size distribution affect the strength of porous ceramics. A smaller pore size and a homogenous pore distribution are thought to be helpful to improve the strength of a porous ceramic. Porous ceramics fabricated through the pore-forming in-situ technique have a high strength, due to their small pore size and well-distributed interconnected pores [9, 11, 17-18, 20-21].

\*Corresponding author:  
Tel : +86-027-68862511  
Fax: +86-027-68862121  
E-mail: yanwenref@yahoo.com.cn

**Table 1.** Chemical compositions of raw materials (wt.%).

	SiO <sub>2</sub>	Al <sub>2</sub> O <sub>3</sub>	Fe <sub>2</sub> O <sub>3</sub>	CaO	MgO	K <sub>2</sub> O	Na <sub>2</sub> O	Ti <sub>2</sub> O	Ignition loss
Talc	44.06	0.14	0.29	0.46	36.27	0.016	0.043	0.041	18.68
Kaolinite gangue	44.7	37.96	0.28	0.08	0.1	0.031	0.39	0.43	15.99
Al(OH) <sub>3</sub>	0.08	64.86	0.06	0.04	0.02	0.04	0.01	-	34.44
Magnesite	1.02	2.51	0.22	0.35	46.3	0.14	0.13	0.14	49.33
Silica	98.7	-	-	-	-	-	-	-	-

**Table 2.** Formulae of seven specimens (wt.%).

	A	B	C	D	E	F	G
Talc	8.27	7.61	7.05	6.56	6.14	5.77	5.44
Kaolinite gangue	16.25	18.63	20.66	22.41	23.94	25.28	26.47
Al(OH) <sub>3</sub>	38.27	39.51	40.57	41.49	42.28	42.98	43.60
Magnesite	12.40	11.41	10.57	9.85	9.21	8.66	8.16
Silica	24.80	22.83	21.14	19.69	18.42	17.31	16.32

**Table 3.** Relative phase contents of specimens sintered at 1430 °C (wt.%).

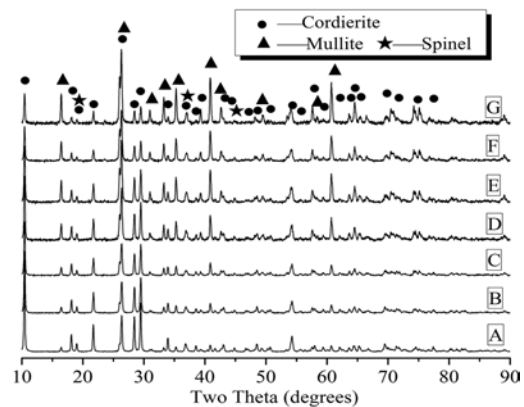
	A	B	C	D	E	F	G
Cordierite	74	63	54	42	33	25	16
Mullite	20	32	42	53	63	71	81
Spinel	6	5	4	5	4	4	3

So, porous cordierite-mullite ceramics with inter-connected pores should be an optimal ceramic filter for the purification of high temperature dusty gas. But until now, porous cordierite-mullite ceramics have not attracted much attention. Although the pore characterization and strength of porous cordierite-mullite ceramics with inter-connected pores prepared by a pore-forming in-situ technique were obtained [11], the strength and gas permeability of porous cordierite-mullite ceramics with different phase compositions and microstructures still has not been fully understood. This will be addressed in the present paper.

## Experimental

Talc, kaolinite gangue, Al(OH)<sub>3</sub>, magnesite, and silica were used as raw materials. The chemical compositions of the raw materials are listed in Table 1. The raw materials were mixed in seven ratios (Table 2), using alumina balls for 3 h. After mixing, the median particle sizes of the powder mixtures B, D and F measured by a laser particle analyzer (Mattersizer 2000) were 23.8 μm, 24.5 μm and 25.7 μm, respectively. The powders were pressed into cylinders with a height of 50 mm and a diameter of 50 mm at a pressure of about 50 MPa, and the green compacts after drying at 110 °C were heated at 1430 °C for 180 minutes in an electric furnace, and then furnace-cooled.

The apparent porosities were measured by the Archimedes' principle with water as the medium. The

**Fig. 1.** X-ray diffraction patterns of specimens sintered at 1430 °C.

closed porosities were calculated based on the apparent porosity and the real density determined by an ACCUPYC 1330. The compressive strengths of sintered specimens were measured at room temperature. Phase analysis was carried out by an X-ray diffractometer (Philips Xpert TMP) with a scanning speed of 2° per minute. In addition, the relative contents of phases in the sintered specimens were evaluated using the standard-free quantitative method [5-6, 9, 11]. The pore size distributions and median pore sizes were obtained by a microscopical measurement method [11, 22] through an optical microscope (Axioskop40). Microstructures were observed by a scanning electron microscope (Philips XL30).

For the measurement of the compressive strength after thermal shock, the sintered specimens were inserted into a preheated furnace at 1100 °C, and then were held there for 25 minutes before they were quenched into a water container which was maintained at 25 °C. Repeat thermal shocks (total 2 cycles) were made. After two thermal shocks, the compressive strengths of the quenched specimens were measured at room temperature. For the measurement of gas permeability, the Chinese national standards of GB/T3000-1999 and the dynamic viscosity of nitrogen gas of  $1.78 \times 10^{-5}$  Pa · s were used [9].

## Results and Discussion

### Phase identification

XRD patterns of specimens sintered at 1430 °C are shown in Fig. 1 and the relative phase contents are listed in Table 3. In all the specimens, the phases are: major cordierite ( $2\text{MgO} \cdot 2\text{Al}_2\text{O}_3 \cdot 5\text{SiO}_2$ ), major mullite

( $3\text{Al}_2\text{O}_3 \cdot 2\text{SiO}_2$ ) and minor spinel ( $\text{MgAl}_2\text{O}_4$ ). With an increase in the content of kaolinite gangue and  $\text{Al}(\text{OH})_3$ , from specimen A to G, the content of cordierite decreases and the content of mullite increases gradually, but the content of spinel change a little.

### Microstructural analysis

Apparent porosities and median pore sizes of specimens are shown in Fig. 2. Specimen B has the highest apparent porosity of 45.5%, specimen G has the lowest apparent porosity of 40.9%, and the difference in their porosities is only 4.6%, which is not very high. But the differences of median pore sizes of specimens are rather distinct. From specimen A to specimen D, the median pore size decreases sharply, but from specimen D to specimen G, the median pore size decreases slightly. The median pore sizes of specimens B, D and F are 179.2  $\mu\text{m}$ , 55.0  $\mu\text{m}$  and 42.3  $\mu\text{m}$ . The closed porosities of specimens B, D and F are 2.2%, 1.5% and 0.8%, respectively.

The pore size distributions of specimens are shown in Fig. 3. Bi-modal pore size distributions are observed in all specimens, and all consist of one higher peak and one lower peak. In the curves of the pore size distribution, peak 1 of the specimens A, B and C are higher, while peak 2 of the specimens D, E, F and G

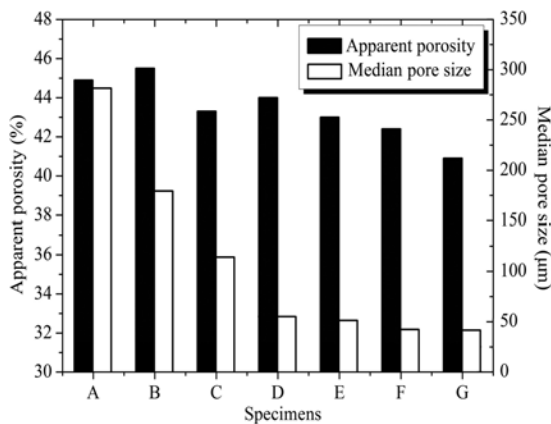


Fig. 2. Apparent porosities and median pore sizes of specimens sintered at 1430 °C.

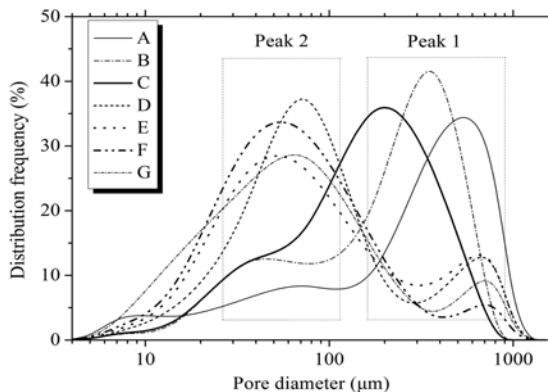


Fig. 3. Pore size distributions of specimens sintered at 1430 °C.

are higher. From specimen A to D, the higher peaks shift largely towards the left; but from specimen D to F, the higher peaks shift slightly, and the peak value of the higher peaks decreases.

In order to investigate the change of the pore distribution, the microstructures of specimens B, D and F are given in Fig. 4. The pores and matrices are distributed homogeneously in the specimens, but the microstructures are rather different. In specimen B, there are a lot of large pores, the small pores are a few; in specimen F, there are a lot of small pores but a few big pores. Comparing specimens B and F, the sizes of pores and grains in specimen B are obviously bigger than those in specimen F. It is clear that the results of the microstructures in Fig. 4 are mostly in accord with those of the pore size distributions in Fig. 3. According to the closed porosities of specimens B, D, and F, it is concluded that the pores are apparent and interconnected.

From the phase identification and microstructural analysis, it is clear that the porous cordierite-mullite ceramics with different phase compositions and an apparent and interconnected porous structure were fabricated successfully.

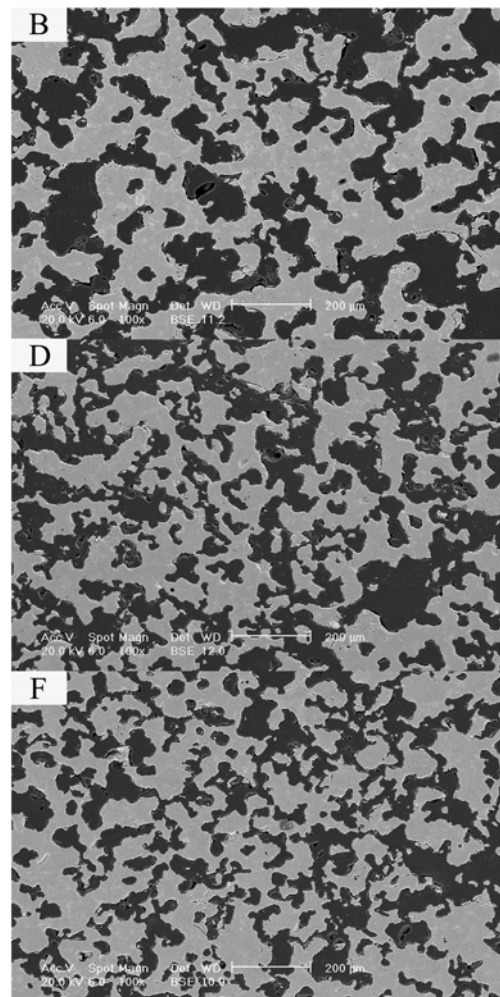
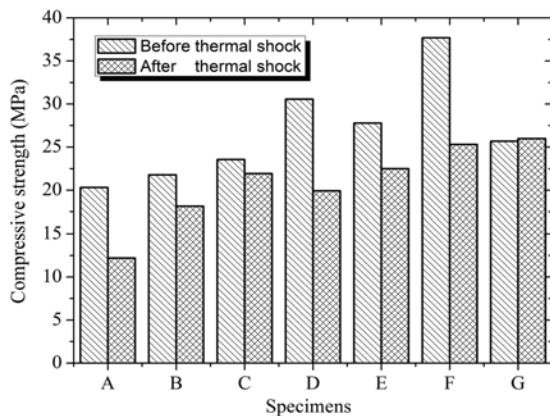
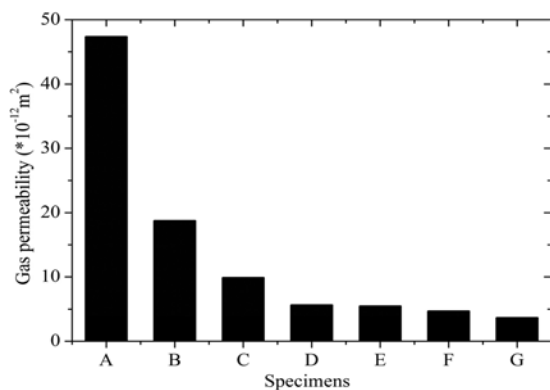


Fig. 4. Microstructures of specimens B, D and F sintered at 1430 °C.



**Fig. 5.** Compressive strengths of sintered specimens before and after thermal shocks.



**Fig. 6.** Gas permeabilities of specimens sintered at 1430 °C.

### Strengths and gas permeabilities

Fig. 5 shows the compressive strengths of the sintered specimens before and after thermal shock. Before thermal shock, from specimen A to specimen D, the compressive strength increases gradually, but from specimen D to specimen G, the compressive strength changes irregularly. The compressive strengths of specimens D and F have the higher values of more than 30 MPa.

After thermal shock, from specimen A to specimen G, the change of the compressive strengths is similar to the change of the compressive strengths of sintered specimens before thermal shock. The compressive strengths of specimens F and G after thermal shock have the higher values of more than 25 MPa, which means that specimens F and G have a higher thermal-shock resistance.

The porosity, median pore size and phase composition strongly affect the strength and the thermal-shock resistance. A small median pore size and an appropriate content of cordierite and mullite help to increase the strength and the thermal-shock resistance, which may be the reason why specimen F has the highest compressive strength and thermal-shock resistance.

Fig. 6 gives the gas permeabilities of the sintered specimens. The sintered specimens all have a high porosity, a large median pore size, an apparent and interconnected pore structure, so they have high gas permeabilities. Specimen A has the highest gas permeability of

$47.35 \times 10^{-12} \text{ m}^2$ . Although the gas permeability of specimen F is relatively small,  $4.68 \times 10^{-12} \text{ m}^2$ , it is still bigger than that ( $4.61 \times 10^{-12} \text{ m}^2$ ) in our earlier work [9]. Comparing the median pore sizes in Fig. 2 with the gas permeabilities in Fig. 6, it is concluded that the median pore size should be the most important factor which affects the gas permeabilities for an apparent and interconnected pore structure. From specimen A to specimen G, the median pore size of sintered specimens decrease, resulting in a decrease of gas permeability.

### Conclusions

Seven porous cordierite-mullite ceramics with different phase compositions and microstructures were fabricated by a pore-forming in-situ technique. The porous cordierite-mullite ceramic consist of 16 ~ 74 wt.% cordierite, 20 ~ 81 wt.% mullite and 3 ~ 6 wt.% spinel. They have high porosities of 40.9 ~ 45.5%, large median pore sizes of 41.6 ~ 281.5  $\mu\text{m}$ , bi-modal pore size distributions, apparent and interconnected pore structures.

The strength, the thermal shock resistance and the gas permeability of the porous cordierite-mullite ceramics with different phase compositions and micro-structures are rather different. When the contents of cordierite are 16 ~ 63 wt.%, the compressive strengths before and after thermal shock are 21.8 ~ 37.7 MPa and 18.1 ~ 26.0 MPa, respectively. Additionally, for the apparent and interconnected pore structure, the gas permeability mainly depends on the median pore size, with an increase in the median pore size from 41.6  $\mu\text{m}$  to 281.5  $\mu\text{m}$ , the gas permeability increases from  $3.65 \times 10^{-12} \text{ m}^2$  to  $47.35 \times 10^{-12} \text{ m}^2$ .

From comprehensive consideration of the porosity, median pore size, gas permeability, strength and thermal-shock resistance, the porous cordierite-mullite ceramic consisting of 25 wt.% cordierite and 71 wt.% has the best performance, which has a high porosity of 42.4%, an appropriate median pore size of 42.3  $\mu\text{m}$ , a high compressive strength of 37.7 MPa, a high thermal-shock resistance and a high gas permeability of  $4.68 \times 10^{-12} \text{ m}^2$ .

### Acknowledgement

The authors would like to thank the Natural Science Foundation of Hubei Province (No. 2011CDB238), the 973 Program earlier research project (No. 2012CB722702), and the Puyang Refractories Co., Ltd for financially supporting this work.

### References

1. M.A. Alvin, Ind. Eng. Chem. Res. 35 (1996) 3384-3398.
2. J. Seville, T.G. Chuah, V. Sibanda, P. Knight, Adv. Powder Technol. 14 (2003) 657-672.
3. J.H. She, T. Ohji, Mater. Chem. Phys. 80 (2003) 610-614.
4. Y.F. Liu, X.Q. Liu, H. Wei, G.Y. Meng, Ceram. Int. 27

- (2001) 1-7.
5. W. Yan, N. Li, B.Q. Han, J. Ceram. Process. Res. 11 (2010) 388-391.
  6. S. Li, N. Li, Ceram. Int. 33 (2007) 551-556.
  7. M. Fukushima, M. Nakata, Y.Y. Wa, J. Ceram. Soc. Jpn. 116 (2008) 1322-1325.
  8. H.M. Alves, G. Tarl, A.T. Fonseca, J.M.F. Ferreira, Mater. Res. Bull. 33 (1998) 1439-1448.
  9. W. Yan, N. Li, B. Han, J. Liu, G. Liu, Trans. Indian Ceram. Soc. 70 (2011) 65-69.
  10. E.M.M. Ewais, Y.M.Z. Ahmed, A.M.M. Ameen, J. Ceram. Process. Res. 10 (2009) 721-728.
  11. W. Yan, H. Luo, J. Tong, N. Li, Inter. J. Mater. Res. 103 (2012) 1239-1243.
  12. E. Ozel, S. Kurama, Ceram. Int. 36 (2010) 1033-1039.
  13. J. Takahashi, M. Natsuisaka, S. Shimada, J. Eur. Ceram. Soc. 22 (2002) 479-485.
  14. T. Ebadzadeh, Brit. Ceram. Trans. 102 (2003) 66-68.
  15. D.N. Boccaccini, C. Leonelli, M.R. Rivasi, M. Romagnoli, A.R. Boccaccini, Ceram. Int. 31 (2005) 417-432.
  16. D.M. Ibrahim, S.M. Naga, Z.A. Kader, E.A. Salam, Ceram. Int. 21 (1995) 265-269.
  17. W. Yan, N. Li, Am. Ceram. Soc. Bull. 85 (2006) 9401-9406.
  18. W. Yan, N. Li, B.Q. Han, Int. J. Min. Met. Mater. 18 (2011) 450-454.
  19. T. Isobe, Y. Kameshima, A. Nakajima, K. Okada, Y. Hotta, J. Eur. Ceram. Soc. 27 (2007) 53-59.
  20. W. Yan, N. Li, Y. Li, G. Liu, B. Han, J. Xu, Bull. Mater. Sci. 34 (2011) 1109-1112.
  21. Y. Wen, L. Nan, B.Q. Han, Am. Ceram. Soc. Bull. 84 (2005) 9201-9203.
  22. N. Li, H. Gu, H. Zhao, in "Refractories Fundamental and Technology", Metallurgical Industry Press (2010) 9.